SPHERICAL DECOMPOSITION OF ARBITRARY SCATTERING GEOMETRIES FOR VIRTUAL ACOUSTIC ENVIRONMENTS

Raimundo Gonzalez *

Department of Computer Science and
Department of Acoustics & Signal Processing
Aalto University
Helsinki, Finland
`raimundo.gonzalezdiaz@aalto.com`

Archontis Politis

Audio Research Group
Tampere University
Tampere, Finland
`archontis.politis@tuni.fi`

Tapio Lokki

Department of Acoustics & Signal Processing
Aalto University
Helsinki, Finland
`tapio.lokki@aalto.fi`

ABSTRACT

A method is proposed to encode the acoustic scattering of objects for virtual acoustic applications through a multiple-input and multiple-output framework. The scattering is encoded as a matrix in the spherical harmonic domain, and can be re-used and manipulated (rotated, scaled and translated) to synthesize various sound scenes. The proposed method is applied and validated using Boundary Element Method simulations which shows accurate results between references and synthesis. The method is compatible with existing frameworks such as Ambisonics and image source methods.

1. INTRODUCTION

Real sound scenes can be quite complex due to the interaction of sound with its physical environment. Methods to reconstruct these complex sound scenes for virtual settings are an active field of research due to an increasing demand on the accuracy of their synthetic representations. Acoustic design and interactive applications, such as room acoustic modeling and Virtual Reality, require better solutions to predict and auralize virtual acoustic scenarios in order to reduce costs and/or enhance immersive experiences.

Virtual Acoustics research has usually focused on some specific element of virtual sound environments. A large, and still growing, corpus of research related to room acoustics modeling exists. Various room acoustic modeling methods have been developed and the main approaches are ray-based modeling [1] and wave-based modeling [2]. In addition to room acoustics modeling, another highly developed topic in virtual acoustics is listener and receiver modeling, which is required for spatial sound listening and capturing. For example, parametric Head-related Transfer Functions (HRTFs) have been proposed [3, 4] as well as wave-based models for receivers [5]. Furthermore, sound sources and their directivity have been modeled through spherical harmonic (SH) decomposition [6] and finite-difference or finite-element methods [7, 8]. In regards to modeling the effects of scattering of entire finite geometries into virtual environments, not much research exists. Though analytical models for basic geometries such as the sphere exist [9], and methods have been proposed to estimate scattering using machine learning [10, 11], still flexible methods for
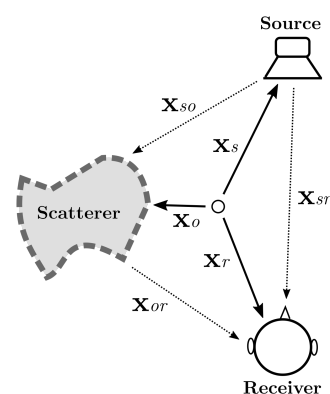
Figure 1: Acoustic scattering scenario

acquiring the scattering properties of arbitrary geometries and integrating them into virtual environments have not yet been explored.

In this paper we propose a method for encoding the scattering properties of entire arbitrary complex geometries through a multiple-input multiple-output (MIMO) spherical decomposition [12, 13] approach of the scattering function. We show how this encoding format is flexible and allows for various manipulations of the scattered field (rotation, scaling, translation). Furthermore, we propose how this format can be easily implemented into existing virtual acoustics frameworks, such as image-source engines and Ambisonics, for applications such as Virtual Reality or Room Acoustic Simulations. Finally, we apply and validate the proposed method using Boundary Element Method (BEM) simulations.

The work extends SH modeling of source [6] or receiver [14] directivities in geometrical acoustics to the doubly directional scattering transfer function of the scattering object. Similar to [8], it assumes a pre-computed wave-based simulation of the radiating field of the object in isolation, before integration into a real-time rendering pipeline. However, contrary to that work where a complicated optimization of multi-pole placement is required, here we decompose the directional scattering directivity into a compact time-invariant matrix of filters, which allows efficient parameterization and manipulation of the scattering object. The simulation stage, which needs to be performed only once for a certain scattering geometry, is implemented using a BEM solver for which free and available implementations exist suitable for acoustical problems [15].

2. GEOMETRIC MODEL

We consider a basic scenario, as seen in Figure 1, of an acoustic source with its acoustic center at position $\mathbf{x}_s$, a scattering object at position $\mathbf{x}_o$, and a receiver at position $\mathbf{x}_r$, from which more complicated scenes can be constructed. Position vectors are defined as

$$\mathbf{x} = [r\cos\theta\sin\phi, r\cos\theta\cos\phi, r\sin\theta] \qquad (1)$$

with r, ϕ and θ corresponding to the spherical coordinates of radial distance, azimuth and elevation. A direction vector on the direction of $\mathbf{x}$ is denoted as $\tilde{\mathbf{x}}$. Additionally, we assume that the source may be directional with directivity function $h_s(f, \tilde{\mathbf{x}}_j)$ dependent on frequency f and radiation direction $\tilde{\mathbf{x}}_j$, while the receiver is also characterized by a directional response vector $\mathbf{h}_r(f, \tilde{\mathbf{x}}_i)$ dependent on direction of arrival $\tilde{\mathbf{x}}_i$, that contain as many directivities as the capturing channels (e.g. two HRTFs in the case of a binaural receiver). Finally, the scattering object is also characterized by a directional scattering function $h_o(f, \tilde{\mathbf{x}}_i, \tilde{\mathbf{x}}_j)$ which depends on both an incident direction-of-arrival $\tilde{\mathbf{x}}_i$ and a scattering direction $\tilde{\mathbf{x}}_j$.

Assuming that source, receiver, and scatterer are all far apart to assume far-field propagation conditions, we can define a simplified geometric model of the received direct sound as typically found in interactive virtual acoustics

$$\mathbf{s}_{r,d}(t) = \frac{1}{||\mathbf{x}_{sr}||} s(t - ||\mathbf{x}_{sr}||/c) * h_s(t, \tilde{\mathbf{x}}_{sr}) * \mathbf{h}_r(t, -\tilde{\mathbf{x}}_{sr}), \quad (2)$$

where $\mathbf{s}_r$ are the receiver time-domain signals, $\mathbf{x}_{sr} = \mathbf{x}_r - \mathbf{x}_s$ the source to receiver vector, c the speed of sound, and $*$ denotes time-domain convolution between the directional filters and the source signal s. In a similar vein we can model the received sound due to the scatterer, as

$$\mathbf{s}_{r,o}(t) = \frac{1}{||\mathbf{x}_{so}|| + ||\mathbf{x}_{or}||} s(t - (||\mathbf{x}_{so}|| + ||\mathbf{x}_{or}||)/c) *$$
$$h_o(t, -\tilde{\mathbf{x}}_{so}, \tilde{\mathbf{x}}_{or}) * \mathbf{h}_r(t, -\tilde{\mathbf{x}}_{or}). \qquad (3)$$

The total sound captured by the receiver due to both the source and scatterer is then, by superposition,

$$\mathbf{s}_r(t) = \mathbf{s}_{r,d}(t) + \mathbf{s}_{r,o}(t). \qquad (4)$$

In this study, we focus on modeling and recovering the scattering filter h_o efficiently to allow dynamic scattering effects integrated in standard interactive virtual acoustics rendering.

3. SCATTERING MODEL

By inscribing the scattering object inside the volume of a sphere of radius R, as presented in Figure 2, we can define the scattered field p_s beyond R as an exterior problem [9]. Making no assumptions on the shape of the object, the scattered sound field pressure $p_s(f, \tilde{\mathbf{x}}_i, \mathbf{x}_j)$ at distance $r = ||\mathbf{x}_j|| \geq R$ from the center of the sphere and direction $\tilde{\mathbf{x}}_j$, due to a unit amplitude plane wave impinging from a direction of arrival $\tilde{\mathbf{x}}_i$, is given by:

$$p_s(f, \tilde{\mathbf{x}}_i, \mathbf{x}_j) = \sum_{n=0}^{\infty} \sum_{m=-n}^{n} C_{mn}(f, \tilde{\mathbf{x}}_i)\, h_n^{(2)}(kr)\, Y_n^m(\tilde{\mathbf{x}}_j) \quad (5)$$

where $k = 2\pi f/c$ is the wavenumber for a frequency f, $h_n^{(2)}$ is the outgoing Hankel function, and Y_n^m is a real spherical harmonic of
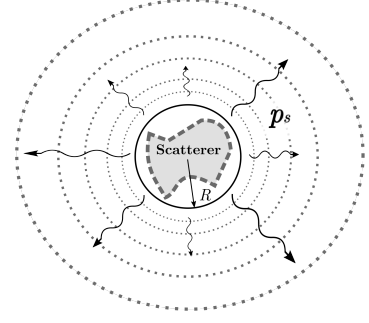

Figure 2: Exterior Problem

order n and degree m. C_{nm} denote modal scattering coefficients that are dependent on frequency and incident direction $\tilde{\mathbf{x}}_i$.

If the continuous scattered pressure over the surface of the surrounding sphere is known, the scattering coefficients C_{mn} can be obtained by the spherical harmonic transform (SHT) of that pressure:

$$C_{nm}(kR, \tilde{\mathbf{x}}_i) = \frac{1}{h_n^{(2)}(kR)} \int_{\tilde{\mathbf{x}} \in S^2} p_s(kR, \tilde{\mathbf{x}}_i, \tilde{\mathbf{x}})\, Y_n^m(\tilde{\mathbf{x}})\, \mathrm{d}A(\tilde{\mathbf{x}})$$
$$(6)$$

where $\mathrm{d}A(\tilde{\mathbf{x}})$ is the spherical surface differential element $\mathrm{d}A(\tilde{\mathbf{x}}) = \cos\theta\mathrm{d}\theta\mathrm{d}\phi$. Note that compared to the preceding formulas the frequency dependency is now integrated into the more representative wavenumber-distance product kR.

In practice, the infinite series of the scattered pressure in Equation (5) is truncated to a maximum order N with negligible error if $N \geq kR$ [16] [17]. Additionally, the C_{mn} scattering coefficients can be recovered through a discrete SHT by a grid $\mathbf{X}_J = [\mathbf{x}_1, ..., \mathbf{x}_J]$ of regularly distributed scattered pressure samples $\mathbf{p}_s = [p_1, ..., p_J]^T$ over the surface of the sphere, where $J \geq (N+1)^2$ and $N \geq kR$. This process can be expressed in a compact form as:

$$\mathbf{c}(kR, \tilde{\mathbf{x}}_i) = \frac{4\pi}{J} \mathbf{D}^{-1}(kR)\, \mathbf{Y}(\tilde{\mathbf{X}}_J)\, \mathbf{p}_s(f, \tilde{\mathbf{x}}_i, \mathbf{X}_J) \qquad (7)$$

where $\mathbf{D}$ is a $(N+1)^2 \times (N+1)^2$ diagonal matrix whose entries are the radial Hankel functions, $\mathbf{y}(\tilde{\mathbf{x}}) = [Y_0^0(\tilde{\mathbf{x}}), ..., Y_N^N(\tilde{\mathbf{x}})]^T$ is a $(N+1)^2$ vector of SH values up to order N, and $\mathbf{Y}(\tilde{\mathbf{X}}_J) = [\mathbf{y}(\tilde{\mathbf{x}}_1), ..., \mathbf{y}(\tilde{\mathbf{x}}_J)]$ is a $(N+1)^2 \times J$ matrix of SH values for the grid directions $\tilde{\mathbf{X}}_J$. Note that, respectively, the coefficient vector $\mathbf{c}$ contains all the coefficients C_{nm} up to order N.

Furthermore, if $\mathbf{c}$ is known for I regularly distributed incident plane wave directions, we can construct a matrix $\mathbf{C}(kR, \tilde{\mathbf{X}}_I) = [\mathbf{c}(\tilde{\mathbf{x}}_1), ..., \mathbf{c}(\tilde{\mathbf{x}}_I)]$ of size $(N+1)^2 \times I$ that contains all the coefficients for the I directions. Subsequently, a discrete SHT can be applied along the incident sphere of directions of the $\mathbf{C}$ matrix as:

$$\mathbf{S}(kR) = \frac{4\pi}{I} \mathbf{C}(kR, \tilde{\mathbf{X}}_I)\, \mathbf{Y}(\tilde{\mathbf{X}}_I)^T. \qquad (8)$$

The resulting $(N+1)^2 \times (N+1)^2$ matrix $\mathbf{S}$ expresses the scattering of the object as a MIMO system [13] between spherical modes of the incident field and spherical modes of the radiating scattered field. It gives a continuous spatially band-limited expression of the scattering at arbitrary directions. In terms of $\mathbf{S}$, the scattered pressure field at point $\mathbf{x}_j$ outside of $R < ||\mathbf{x}_j||$ is expressed by:

$$p_s(f, \tilde{\mathbf{x}}, \mathbf{x}_j) = \mathbf{y}(\tilde{\mathbf{x}}_j)^T\, \mathbf{D}(kr)\, \mathbf{S}(kR)\, \mathbf{y}(\tilde{\mathbf{x}}_i) \qquad (9)$$

Finally, assuming an adequate distance between the scatterer and receiver such that the Hankel function in Equation (9) converge to a far-field spherical wave [9], the simple scattering filter of Equation (3) is given by:

$$p_s(f, \tilde{\mathbf{x}}_i, \mathbf{x}_j) = \mathbf{y}(\tilde{\mathbf{x}}_j)^T \mathbf{S}(kR) \, \mathbf{y}(\tilde{\mathbf{x}}_i) \qquad (10)$$

The scattering matrix $\mathbf{S}$ of an object can be manipulated in various ways for multiple virtual acoustics scenarios.

3.1. Scattering Model to Geometric Model

If the scattered pressure p_s is the product of unit amplitude plane waves, the time domain scattering filter h_o from Section 2 can be recovered, for far-field sources, using the inverse Fourier Transform of p_s.

4. MANIPULATIONS

The proposed scattering format of Equation (8) allows for flexible manipulations of the scattered field. The scattering matrix $\mathbf{S}$ allows for a series of transformation to rotate, scale and translate an initial scattering scenario.

4.1. Rotation

Obtaining the filter for a rotated scatterer can be efficiently performed in two ways. The first is by rotating the geometry of the scatterer, while the second is by performing the rotation in the spherical harmonic domain (SHD). We define the three Euler angles α, β, γ corresponding to e.g. the yaw-pitch-roll convention, and the respective 3×3 rotation matrix $\mathbf{M}_{\mathrm{ypr}}(\alpha, \beta, \gamma)$. The scattering pressure for the rotated object is then given by:

$$p_s(f, \mathbf{M}_{\mathrm{ypr}}\tilde{\mathbf{x}}_i, \mathbf{M}_{\mathrm{ypr}}\mathbf{x}_j) =$$
$$= \mathbf{y}(\mathbf{M}_{\mathrm{ypr}}\tilde{\mathbf{x}}_j)^T \mathbf{D}(kr)\mathbf{S}(kR)\mathbf{y}(\mathbf{M}_{\mathrm{ypr}}\tilde{\mathbf{x}}_i) \qquad (11)$$

Alternatively, the rotation can be performed using $(N+1)^2 \times (N+1)^2$ SHD rotation matrices $\mathbf{M}_{\mathrm{shd}}(\alpha, \beta, \gamma)$, which can be computed very efficiently based on $\mathbf{M}_{\mathrm{ypr}}(\alpha, \beta, \gamma)$ and recursive relationships [18]. The rotated scattering is then:

$$p_s(f, \mathbf{M}_{\mathrm{ypr}}\tilde{\mathbf{x}}_i, \mathbf{M}_{\mathrm{ypr}}\mathbf{x}_j) =$$
$$= \mathbf{y}(\mathbf{M}_{\mathrm{ypr}}\tilde{\mathbf{x}}_j)^T \mathbf{D}(kr)\mathbf{S}(kR)\mathbf{y}(\mathbf{M}_{\mathrm{ypr}}\tilde{\mathbf{x}}_i) =$$
$$\mathbf{y}(\tilde{\mathbf{x}}_j)^T \mathbf{M}_{\mathrm{shd}}^T \mathbf{D}(kr)\mathbf{S}(kR)\mathbf{M}_{\mathrm{shd}}\mathbf{y}(\tilde{\mathbf{x}}_i). \qquad (12)$$

Even though rotating the incident and scattering vectors would be normally more efficient, rotation in the SHD can be applied also in the case that the incident sound field is not a single plane wave, but a plane wave distribution, e.g. as described in Sec. 5.2.

4.2. Translation

Analytical translation of sound fields can be based on expansions similar to the exterior problem of Equation (2) and related addition/translation theorems, e.g. as found in multi-sphere scattering [19]. However, we avoid the complexity of such solutions and focus on the simple geometric transformation that fit the interactive scenario under consideration. For a translation given by vector $\mathbf{x}_t$ of the center of the scattering center, the source-to-object $\mathbf{x}_{so}$ and object-to-receiver vectors $\mathbf{x}_{or}$ are updated accordingly:

$$\mathbf{x}'_{so} = \mathbf{x}_{so} + \mathbf{x}_t \quad \text{and} \quad \mathbf{x}'_{or} = \mathbf{x}_{or} + \mathbf{x}_t. \qquad (13)$$

The updated position vectors can be used to simulate the attenuation/amplification due to the changes in distance and angle between source, scatterer, and receiver by updating Equation (3).

4.3. Scaling

The matrix $\mathbf{S}$ can be reused to simulate the scaling of the size of the scattering object under the following assumptions:

1. Though the scattered pressure of a geometry is initially decomposed for a sphere of radius R and wavenumber k, the final matrix $\mathbf{S}$ is solely dependent on kR and is agnostic of the initial radius-to-wavenumber transformation ratio.
2. Scaling the radius R of the sphere enclosing the scattering object will have a proportional effect on the size of the scattering object itself.
3. If the radius of decomposition R is scaled to some R', the matrix $\mathbf{S}$ still contains all the necessary coefficients to reconstruct the scattered pressure at a point $r \geq R'$, as long $k'R' = kR$, where k' is the scaled wavenumber of the original k.

In other words, a matrix $\mathbf{S}$ can be used to simulate the scattered field of a bigger version of the initial geometry at a lower frequency as long as the initial kR quantity is maintained [16].

5. VIRTUAL ACOUSTIC INTEGRATION

Image-source techniques and Ambisonics can be used with the proposed method to produce early and late stages of scattering reverberation within a room.

5.1. Image-Source Method

For virtual acoustic scenarios which make use of an image-source method, the translation and rotation manipulations of Equations (12) and (13) can be used multiple times to simulate the early reflections of the scattered field inside a room [1]. Starting with the simple case of a single wall shown Figure 3, the reflection of the scattered field against the wall can be simulated as a second "image scatterer". The position of the second scatterer will be mirroring (translation and rotation) the position of the initial scatterer with respect to the wall. The same process can be applied for a room with several walls as well as for higher-order reflections.
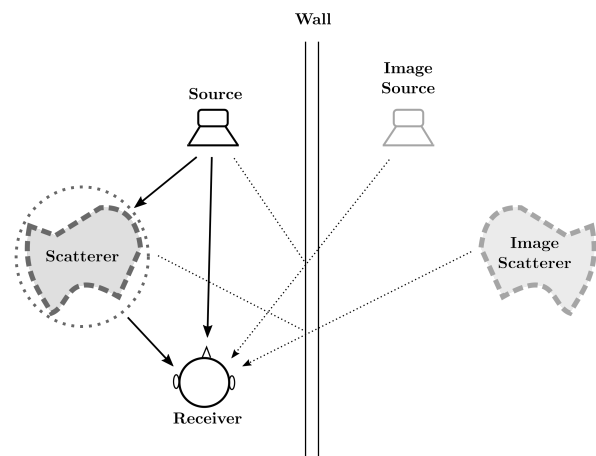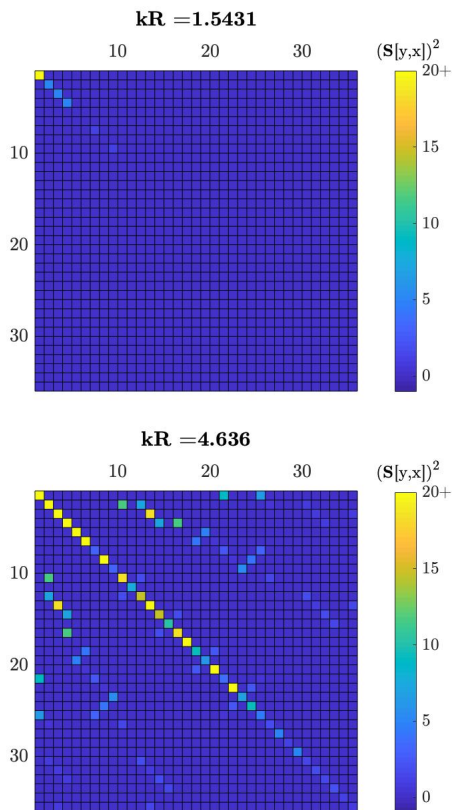

Figure 3: Image source-scatterer scene

Figure 4: Energy of a matrix $\mathbf{S}$ from encoding a 50 cm sided cube for two frequencies

Figure 5: Normalized energy integration per order. Dashed lines indicate a 0.95 threshhold

rule, the number of coefficients in a matrix $\mathbf{S}$ required to synthesize a scattering field is much lower at low frequencies than at high frequencies. This is reflected in the energy of the components of the matrix which, as seen as Figure 4, is usually highest towards the first components, $\mathbf{S}[1, 1]$, and lower in energy towards its bottom-right components.

Therefore, rows and columns from the bottom right of the matrix can be discarded to reduce the storage size and/or processing time. An efficient approach to defining coefficients to be dismissed is to integrate the normalized energy of the matrix, order by order, and define a threshold after which the coefficients are discarded. Figure 5 indicates how a matrix $\mathbf{S}$ reaches its maximum normalized energy at different rates. An example threshold of 0.95 is denoted with dotted lines after which matrix coefficients could be discarded. In conjunction with a frequency-dependent order-limitation, the matrix can be also highly sparse, depending on smoothness and symmetries in the scattering directivity, with only a few entries contributing to it. In this case its storage requirements can be further reduced, using sparse matrix processing techniques.

5.2. Scattering of Ambisonic signals

Another case of interest, for interactive scattering acoustic environments, is the case that we have a continuous description of the incident field at the scattering center, expressed in the SH domain, and normally captured or modeled in terms of ambisonic signals $\mathbf{a}(t)$, up to order L. Such signals, for example, may be modeling the combined contribution of late reverberation at the scattering position, generated through a spatial reverberator [20]. It is still possible to compute the scattering at $\mathbf{x}_j$ due to such incidence simply by:

$$p_s(f, \mathbf{a}, \mathbf{x}_j) = \mathbf{y}(\tilde{\mathbf{x}}_j)^T \mathbf{D}(kr) \mathbf{S}(kR) \mathbf{a}(f). \tag{14}$$

Since it may be that the order of the incident ambisonic signals is lower than the scattering order coming from simulation $L < N$, the scattering matrix $\mathbf{S}$ may have to be truncated to $(N + 1)^2 \times (L + 1)^2$.

6. OPTIMIZATIONS

Encoded scattering matrices $\mathbf{S}$ acquired through the proposed method can also be optimized to reduce memory storage as well as computations during run-time. A scattering matrix containing multiple frequencies is order-limited. Following the $N \geq kR$ [16]
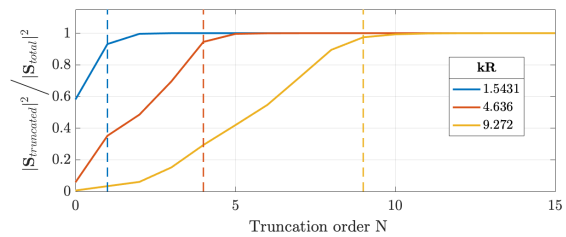
7. SIMULATION

As an example for the proposed method, the scattered field of a 50 cm sided rigid cube (Figure 6) was simulated using the Boundary-Element Method (BEM) module of COMSOL Multiphysics [21]. The cube was chosen as an example geometry for it is a quite standard shape that has hard edges capable of producing complex scattering patterns. The incident field for the simulations were far-field plane-waves that were removed from the final scattered sound field. Figure 7 presents a visualization of the total pressure field, incident and scattered, for a single planewave and Figure 8 presents a directivity plot of the isolated scattering pressure from the surface of the geometry. The field was simulated for 64 frequencies from 78 Hz to 5 kHz for 1200 incident directions following a 48th degree spherical T-design arrangement, suitable for an up to 24th order SH decomposition. The scattered sound pressure around the cube was then sampled for the same 1200 directions at 37 cm away from the origin as presented in Figure 9. For the meshing in the BEM simulation, a free quadrilateral mesh was used with a spatial resolution of $\frac{1}{6}$ of the wavelength of the simulated frequency [21] as shown in Figure 6. The simulations were run using Triton, Aalto University's high-performance computer cluster. The simulated scattered pressures were then exported, organized and processed in Matlab. The scattering
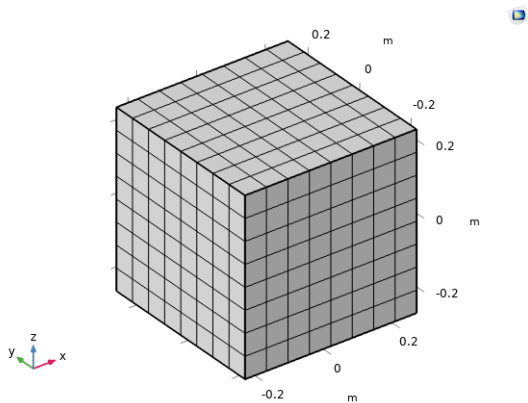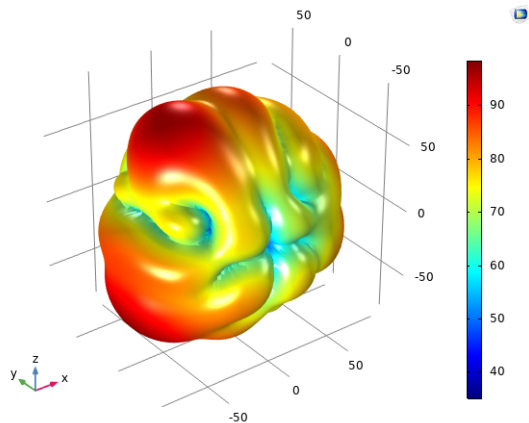
Figure 6: Mesh of simulated cube at 1 kHz

Figure 8: Directivity of scattered sound pressure level over surface of cube, for an incident 1 kHz plane wave incoming from $0°$ azimuth and $40°$ elevation
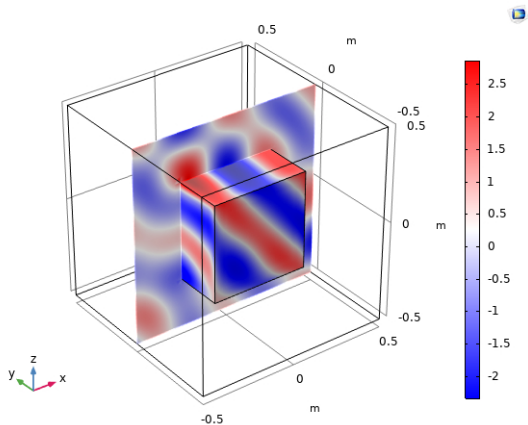

Figure 7: Total pressure over surface of cube, and cross sectional area along x-axis, for an incident 1 kHz plane wave incoming from $0°$ azimuth and $40°$ elevation

coefficients C_{nm} for each incident direction were recovered using Eq. 7 and then organized as a matrix $\mathbf{C}$ to recover the scattering matrix $\mathbf{S}$ through Eq. 8.

8. VALIDATION

To test the scattering matrix generated from the previous section, comparisons were made between scattered pressure synthesized through the matrix and reference BEM simulations, see Figure 10. First, comparisons were made with a cube of same dimensions, for a direction $\tilde{\mathbf{x}}_j = (0, 0)$ which was not in the original 1200 directions. Then, the same cube was rotated in two directions, $(\alpha, \beta, \gamma) = (45, -55, 0)$. Finally, the previously rotated cube was also scaled up by 50% or $R' = 1.5 \times R$. For all cases, the scattered field was sampled at 3 positions which capture the pressure diversity of the field.

As seen in Figure 10, the pressure for the reference and synthe-
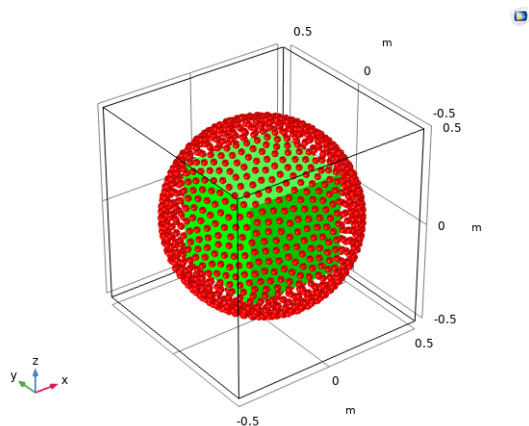

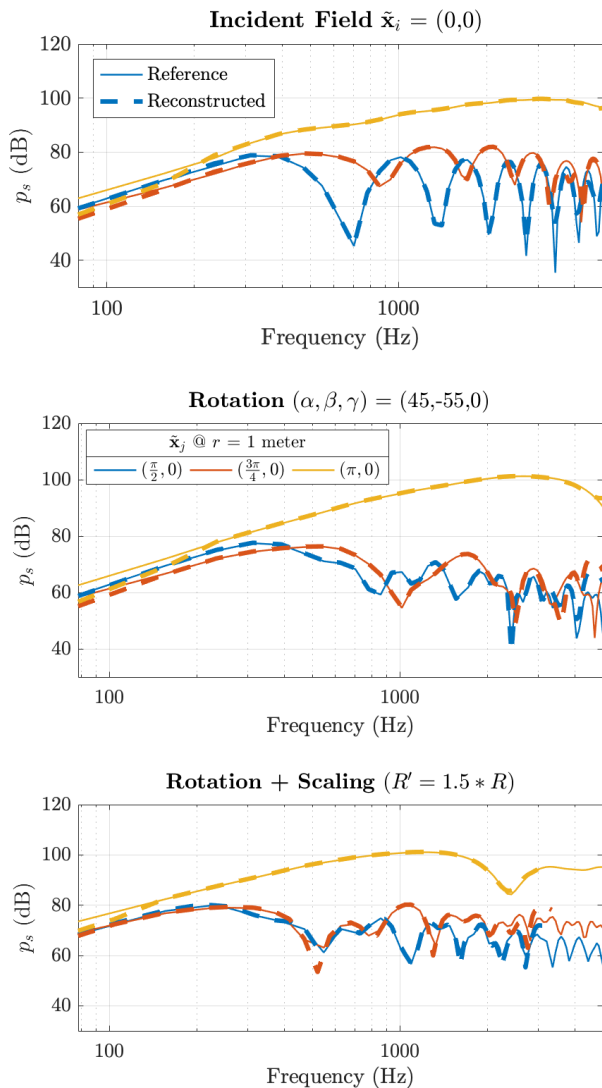Figure 9: Sampling points around target geometry

Figure 10: Comparison of scattered pressure between reference and synthesis for 3 scattering directions indicated by colors. **Top**: 50 cm cube **Middle**: Previous cube with rotation. **Bottom**: Previous rotated cube scaled up by 50%.

sized pressure match appropriately. Towards the higher frequencies of the synthesis, mismatches occur with the reference due to the effects of aliasing. This would be solved by increasing the order of the T-design used to excite and probe the scattering of the geometry. As expected, the maximum frequency synthesized for the rotation + scaling example is lower, 3177 Hz instead of 5 kHz, due to the enlargement of the geometry.

9. FUTURE WORK

Further work is required to validate the accuracy of the proposed method for other more complex geometries as well as against real acoustic measurements. Also, the perceptual impact of the error from truncating the scattering matrix at lower orders should be studied to define a practical and acceptable rendering resolution. Finally, optimizations to reduce the size of the scattering matrix should be explored to achieve real time implementations of sound scattering in interactive environments.

10. CONCLUSIONS

The scattering of a finite arbitrary object can be encoded in the spatial frequency domain if sufficient incident fields and sampling points in spherical coordinates are known. The encoded scattering can be contained in a matrix, allows for various manipulations of the geometry in space, and can be reused to create more complex virtual acoustic scenarios. The encoded scattering matrix can be optimized to reduce its memory storage as well as processing runtime. A simulation environment can be used to acquire a scattering matrix that can be reused, producing accurate results.

11. ACKNOWLEDGMENTS

12. REFERENCES

[1] L. Savioja and U. P. Svensson, "Overview of geometrical room acoustic modeling techniques," *The Journal of the Acoustical Society of America*, vol. 138, no. 2, pp. 708–730, 2015.

[2] S. Bilbao, "Modeling of complex geometries and boundary conditions in finite difference/finite volume time domain room acoustics simulation," *IEEE Transactions on Audio, Speech, and Language Processing*, vol. 21, no. 7, pp. 1524–1533, 2013.

[3] R. O. Duda and W. Martens, "Range-dependence of the HRTF of a spherical head," 1997, vol. 104, p. 5 pp.

[4] G. Ramos and M. Cobos, "Parametric head-related transfer function modeling and interpolation for cost-efficient binaural sound applications," *The Journal of the Acoustical Society of America*, vol. 134, no. 3, pp. 1735–1738, 2013.

[5] S. Bilbao, A. Politis, and B. Hamilton, "Local time-domain spherical harmonic spatial encoding for wave-based acoustic simulation," *IEEE Signal Processing Letters*, vol. 26, pp. 617–621, 2019.

[6] M. Noisternig, F. Zotter, and B. Katz, "Reconstructing sound source directivity in virtual acoustic environments," in *Principles and Applications of Spatial Hearing*, pp. 357–372. World Scientific, 2011.

[7] S. Bilbao and J. Ahrens, "Modeling continuous source distributions in wave-based virtual acoustics," *The Journal of the Acoustical Society of America*, vol. 148, no. 6, pp. 3951–3962, 2020.

[8] D. L. James, J. Barbič, and P. K. Dinesh, "Precomputed acoustic transfer: output-sensitive, accurate sound generation for geometrically complex vibration sources," *ACM Transactions on Graphics (TOG)*, vol. 25, no. 3, pp. 987–995, 2006.

[9] E. G. Williams, *Fourier Acoustics*, Academic Press, Cambridge, MA, 1999.

[10] V. Pulkki and U. P. Svensson, "Machine-learning-based estimation and rendering of scattering in virtual reality," *The Journal of the Acoustical Society of America*, vol. 145, no. 4, pp. 2664–2676, 2019.

[11] Z. Fan, V. Vineet, HJ. Gamper, and N. Raghuvanshi, "Fast acoustic scattering using convolutional neural networks," in *ICASSP 2020-2020 IEEE International Conference on Acoustics, Speech and Signal Processing (ICASSP)*. IEEE, 2020, pp. 171–175.

[12] H. Morgenstern, B. Rafaely, and F. Zotter, "Theory and investigation of acoustic multiple-input multiple-output systems based on spherical arrays in a room," *The Journal of the Acoustical Society of America*, vol. 138, no. 5, pp. 2998–3009, 2015.

[13] H. Morgenstern, B. Rafaely, and M. Noisternig, "Design framework for spherical microphone and loudspeaker arrays in a multiple-input multiple-output system," *The Journal of the Acoustical Society of America*, vol. 141, pp. 2024–2038, 2017.

[14] G. D. Romigh, D. S. Brungart, R. M. Stern, and B. D. Simpson, "Efficient real spherical harmonic representation of head-related transfer functions," *IEEE Journal of Selected Topics in Signal Processing*, vol. 9, no. 5, pp. 921–930, 2015.

[15] V. C. Henriquez and P. M. Juhl, "OpenBEM –an open source boundary element method software in acoustics," in *Proceedings of Internoise 2010*, 2010.

[16] D. B. Ward and T. D. Abhayapala, "Reproduction of a plane-wave sound field using an array of loudspeakers," *IEEE Transactions on Speech and Audio Processing*, vol. 9, no. 6, pp. 697–707, 2001.

[17] S. Moreau, J. Daniel, and S. Bertet, "3D sound field recording with higher order ambisonics - objective measurements and validation of a 4th order spherical microphone," in *Proc. 120th Convention of the AES*, 2006, pp. 20–23.

[18] J. Ivanic and K. Ruedenberg, "Rotation matrices for real spherical harmonics. direct determination by recursion," *The Journal of Physical Chemistry A*, vol. 102, no. 45, pp. 9099–9100, 1998.

[19] N. A. Gumerov and R. Duraiswami, *Fast Multipole Methods for the Helmholtz Equation in Three Dimensions*, Elsevier, 2004.

[20] Benoit Alary, Archontis Politis, Sebastian Schlecht, and Vesa Välimäki, "Directional feedback delay network," *Journal of the Audio Engineering Society*, vol. 67, no. 10, pp. 752–762, 2019.

[21] COMSOL Multiphysics, "Acoustics module user's guide," pp. 140–154, 2020.